Investigation of structural-scale levels of spall fracture induced by a nanosecond relativistic high-current electron beam in ultrafine-grained Ti–Al–V–Mo alloy

E. F. Dudarev, A. B. Markov, G. P. Bakach, T. Yu. Maletkina, N. N. Belov, A. N. Tabachenko, A. B. Skosirskii, M. V. Habibullin, and E. V. Yakovlev

Citation: AIP Conference Proceedings **1909**, 020036 (2017);
View online: https://doi.org/10.1063/1.5013717
View Table of Contents: http://aip.scitation.org/toc/apc/1909/1
Published by the American Institute of Physics

Investigation of Structural-Scale Levels of Spall Fracture Induced by a Nanosecond Relativistic High-Current Electron Beam in Ultrafine-Grained Ti–Al–V–Mo Alloy

E. F. Dudarev[1,a)], A. B. Markov[2,b)], G.P. Bakach[1], T. Yu. Maletkina[1,3,c)], N. N. Belov[1], A. N. Tabachenko[1], A. B. Skosirskii[1], M. V. Habibullin[1], and E. V. Yakovlev[2]

[1] *National Research Tomsk State University, Tomsk, 634050 Russia*
[2] *Institute of High Current Electronics SB RAS, Tomsk, 634055 Russia*
[3] *Tomsk State University of Architecture and Building, Tomsk, 634003 Russia*

[a)] Corresponding author: dudarev @spti.tsu.ru
[b)] almar@Lve.hcei.tsc.ru
[c)] t.maletkina@yandex.ru

Abstract. The results of an experimental and theoretical study of shock-wave processes and spall fracture in an ultrafine-grained and coarse-grained ($\alpha+\beta$) Ti–Al–V–Mo alloy under the action of a nanosecond relativistic high-current electron beam are reported. Mathematical modeling is performed to show that when an electron beam with a power density of 1.65×10^{10} W/cm^2 impacts this alloy, a shock wave with a compression amplitude of 13 GPa appears and its reflection gives rise to a tensile wave. Its amplitude increases with decreasing target thickness. The calculated increase in the thickness of the spalled layer at the rear surface of the target corresponds to the experimental data. It is established experimentally that plastic deformation precedes the spall fracture sequentially at three structural-scale levels. At the beginning pores are formed and merge, then microcracks are formed at different angles to the back surface of the target between the pores, and then a macrocrack is formed. As a result, the macrocrack surface is not smooth but exhibits pits of ductile fracture.

INTRODUCTION

Four-component Ti–4% Al–1% V–3% Mo (wt %) titanium alloy with ($\alpha+\beta$) structure is widely used in aerospace industry as a structural and functional material for the production of parts. A significant improvement in its mechanical properties at strain rates below 10^{-1} s^{-1} and creep was achieved as a result of coarse-grained structure refinement to ultrafine-grained one by severe plastic deformation with preserving the heterophase structure [1, 2]. In some cases, parts made of this alloy are subjected to shock-wave loads.

However, a comprehensive research of the effect of transformation from the coarse-grained to ultrafine-grained structure on the deformation behavior and spall fracture at different structural-scale levels in the conditions of shock-wave loading have not yet been performed.

Recently, nanosecond relativistic high-current electron beams which could provide electron penetration into a metal target up to a depth of 1 mm have been used along with common methods of dynamic impact to study shock-wave processes and spallation phenomena. This allowed the investigation of the spall fracture regularities and mechanisms for massive targets of different thickness.

The present work performs an experimental and theoretical study of shock-wave processes, features and mechanisms of spall fracture at different structural-scale levels of Ti–4% Al–1% V–3% Mo alloy under the impact of

Proceedings of the International Conference on Advanced Materials with Hierarchical Structure for New Technologies and Reliable Structures 2017 (AMHS'17)
AIP Conf. Proc. 1909, 020036-1–020036-4; https://doi.org/10.1063/1.5013717
Published by AIP Publishing. 978-0-7354-1601-7/$30.00

a nanosecond relativistic high-current electron beam. Targets have the same thickness and identical chemical composition for both ultrafine-grained and coarse-grained structures.

RESULTS AND DISCUSSION

A physico-mathematical model [3–6] and a calculation method [7, 8] in the axisymmetric geometry were used for the simulation of shock-wave processes and spall fracture in heterophase Ti–4% Al–1% V–3% Mo alloy with the following electron beam parameters: electron energy 1.4 MeV, pulse duration 50 ns, average power density 1.65×10^{10} W/cm^2, linear absorption coefficient of electrons 46 cm^{-1}, and electron beam diameter 60 mm.

The initial density of the alloy $\rho_0 = 4.52$ g/cm^3, the volume velocity of sound $C_0 = 5.11$ km/s, the shear modulus $G = 42.62$ GPa, and the yield stress under dynamic loading $\sigma_S = 0.4$ GPa were used as the characteristics of the physical and elastoplastic properties of the target material. At the same time, it was assumed that the pore volume reaches a critical value of 0.3, which is usually used in ductile fracture modeling under shock wave loading as a criterion for the onset of spall fracture.

According to the calculations, the melting and burst of the target material from the molten layer takes place in the zone of the electron beam and further the field of the vectors of mass velocity changes (Fig. 1). The thickness of the molten layer reaches 0.6 mm and a high-pressure zone with a maximum compressive stress of 18.5 GPa appears at a distance of about 0.3 mm from the interface between the solid and liquid phases (Fig. 2).

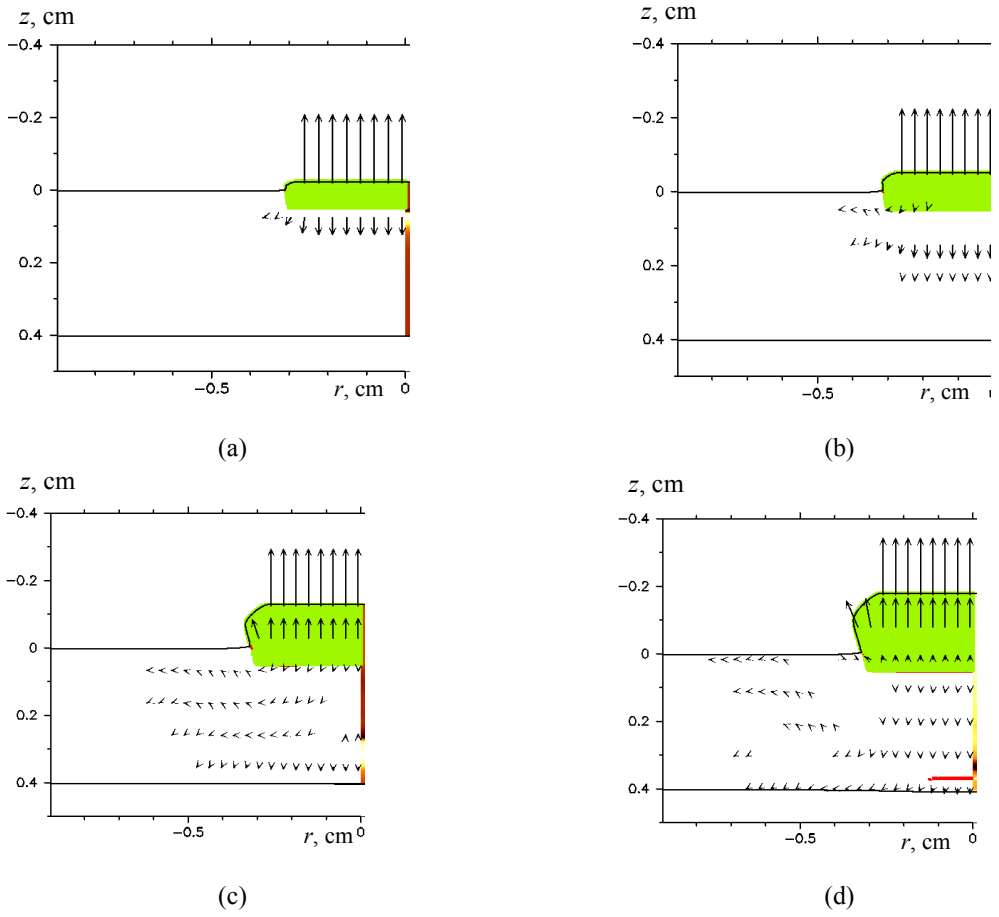

FIGURE 1. A chronogram of 4-mm thick target irradiation: the field of mass velocity vectors and the zone of molten alloy after 150 (a), 300 (b), 750 (c) and 1050 ns (d) from the onset of electron beam irradiation, where z is the distance from the target surface and r is the target radius

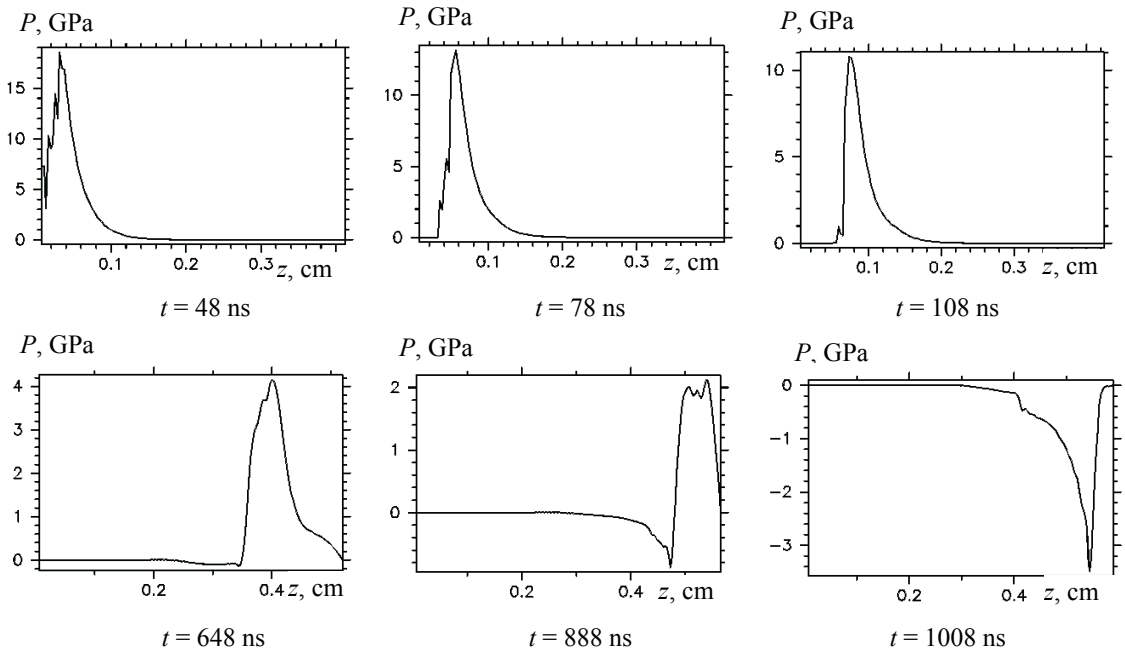

FIGURE 2. Shock wave and tensile wave at different instants of time t from the beginning of electron beam irradiation of the target, where *P* is the stress and *z* is the distance from the target surface

Then a shock wave with an amplitude of 13 GPa forms in the solid phase. When the shock wave propagates to the rear surface, its amplitude and mass velocity decrease. At a distance of 4 mm from the front surface, the amplitude becomes 4 GPa, and the mass velocity is less by 200 m/s.

The reflection of the shock wave from the rear surface leads to the appearance of a tensile wave (Fig. 2). Following the shock wave, a wave of unloading emerges on the surface. From this moment, the tensile stress distribution, which takes place on the rear surface, is determined by the interaction of the tensile wave and the unloading wave. The distance from the rear surface at which the acting tensile stress reaches the spall strength rises with increasing thickness of the target. Herewith the dependence of the spalled layer thickness on the target thickness is close to linear. In the process of failure, the tensile stress rapidly relaxes to zero and a compression wave appears in the tensile zone, which emerges on the surface in the form of a spall pulse. It is approximately 0.8 GPa in a target of thickness 4 mm.

A heat affected zone with a large temperature gradient appears near the melt zone. Since the front velocity of the heat affected zone is much lower than the shock wave velocity, spall fracture locates outside the heat affected zone in targets of thickness 2 mm and more.

For experimental research of spall fracture, disks of thickness 2, 3, 4 and 5 mm were used as targets for electron beam irradiation. The disks had an isotropic coarse-grained or ultrafine-grained structure with an average grain size of 600 and 0.8 μm, respectively. Before irradiation, the initial coarse-grained structure was heterophase and consisted of α-phase plates with a thickness of up to 5 μm and a β-phase with a thickness of less than 0.5 μm. During ultrafine-grained structure formation in the process of warm *abc*-pressing, the β-phase plate structure turned into a lamellar-globular structure, and the crystallographic texture remained "gray". These changes in the structural-phase state at the formation of ultrafine structures led to an increase in the flow stress and fracture under quasi-static tension. The fracture mechanism remained ductile-brittle with shallow pits of rupture in the presence of a small number of facets of quasi-spall, but the diameter of the shallow pits decreased.

The irradiation of targets with both grain structures was carried out at the same parameters of the electron beam, which were given above. At a single irradiation pulse irrespectively of the target thickness and its grain structure, one spall is formed on the irradiated (front) surface with coarse-grained structure and two spall cracks with ultrafine-grained structure.

The formation of pores precedes the appearance of the main crack and subsequent formation of microcracks at different angles to the rear surface of the target. Thus, the continuity violation in the target material on the nanoscale

(pores) and microscale (microcracks) levels precedes the formation of the main crack. The length of microcracks and the distance between them in the alloy with coarse-grained structure is several times larger than that for ultrafine-grained structure. As fracture develops at three structural-scale levels, the spall surfaces are not smooth. According to the definition in the scientific literature, they are rough and consist of crests and troughs [3, 4, 8].

The spalled layer thickness increases in the alloy with coarse-grained and ultrafine-grained structures and the value of its plastic deformation decreases with increasing target thickness. For example, increasing the target thickness from 2 to 3 mm resulted in an increase in the spalled layer thickness from ~0.2 to ~0.4 mm in the alloy with ultrafine-grained structure. For the target of thickness 4 or 5 mm, main cracks did not occur from the rear surface.

Spall fracture is ductile-brittle fracture with pits of ductile rupture and quasi-facets of spall in the alloy with coarse-grained and ultrafine-grained structures similarly to fracture with the strain rate of 10^{-3} s^{-1}. However, the depth of rupture pits for spall fracture (strain rate 10^{5} s^{-1}) is much larger than that at a strain rate of 10^{-3} s^{-1}. At the same time, the diameter of pits of rupture and their depth in the alloy with ultrafine-grained structure is smaller than that for coarse-grained structure. The surface of pits of rupture exhibits a large numbers of pores.

CONCLUSIONS

The experimental and theoretical study results for spall fracture in Ti-Al-V-Mo alloy with ultrafine-grained and coarse-grained structures under the influence of a nanosecond electron beam were reported which indicate the development of successive damage on three structural-scale levels. A nonsmooth fracture surface (presence of crests and troughs on the mesoscale level) is a consequence of microcracking in front of the propagating macrocrack. Finally, the grain size in the alloy with the initial coarse-grained structure in the spalled zone decreases to ultrafine, and the β-phase morphology changes from lamellar to globular. In the alloy with the initial ultrafine-grained structure the grain size does not change, but the β phase presented by lamellar-globular structure in the initial target transforms to a globular one.

ACKNOWLEDGMENTS

The work was carried out with the financial support of the Russian Foundation for Basic Research within Project No. 15-08-04118.

REFERENCES

1. Yu. R. Kolobov, R. Z. Valiev, and G. P. Grabovetskaya, et al., *Grain Boundary Diffussion and Properties of Nanostructured Materials* (International Science Publishing, Cambridge, 2007).
2. R. Z. Valiev and I. V. Aleksandrov, *Bulk Nanostructured Metallic Materials: Production, Structure and Properties* (IKC Akademkniga, Moscow, 2007).
3. G. J. Kanel, S. V. Razorenov, A. V. Utkin, and V. E. Fortov, *Shock-Wave—Wave Phenomena in Condensing Environments* (Ianus-K, Moscow, 1996).
4. T. Antoun, L. Seaman, D. R. Currant, et al., *Spall Fracture* (Springer-Verlag, New York, 2003).
5. E. F. Dudarev, O. A. Kashin, and A. B. Markov, et al., Russ. Phys. J. **54**, 713 (2011).
6. E. F. Dudarev, S. A. Afanasyeva, G. P. Bakach, et al., Russ. Phys. J. **57**, 1464 (2014).
7. M. V. Habibullin and S. A. Afanasyeva, *Program for Calculation of the Phenomena Occurring in Condensed Matter as a Result of Intensive Pulsed Effects in Axisymmetric Position*, Certificate No. 2012617301 (Moscow, 2012).
8. E. F. Dudarev, A. B. Markov, G. P. Bakach, T. Yu. Maletkina, et al., AIP Conf. Proc. **1783** (American Institute of Physics, Melville, NY, 2016), pp. 020047-1–020047-4.